ABSTRACT

Title of Thesis: SURFACE ACOUSTIC WAVE (SAW) PROPAGATION IN NANOSTRUCTURED DEVICES

KEZHEN XU,
Master of Science, 2019

Thesis Directed By: Professor Agis Iliadis
Department of Electrical and Computer Engineering

$ZnO/SiO_2/Si$ surface acoustic wave Love mode sensors are considered to be promising high sensitivity sensors. Previous research has tested $ZnO/SiO_2/Si$ SAW sensors with selected operating frequency and guiding layer thickness. This investigation is based on experimental data of previous research and used the theories and equations from that research to evaluate and develop a model of the mass sensitivity of surface acoustic wave (SAW) devices with two different piezoelectric semiconductors, $ZnO/SiO_2/Si$ and $GaN/SiO_2/Si$ Love mode SAW sensors. The SAW mass sensitivity model developed here, examined the mass sensitivity of the SAW device with respect to the design parameters, like wavelength, piezoelectric layer thickness, and the two different semiconductors (ZnO, and GaN) to obtain optimum mass sensitivity. The mass sensitivity increases when the wavelength is increasing. The model also shows that the maximum mass sensitivity of GaN-based devices is 10% better than the maximum mass sensitivity of ZnO-based devices.

SURFACE ACOUSTIC WAVE (SAW) PROPAGATION IN NANOSTRUCTURED DEVICES

by

Kezhen Xu

Thesis submitted to the Faculty of the Graduate School of the
University of Maryland, College Park, in partial fulfillment
of the requirements for the degree of
Master of Science
2019

Advisory Committee:
Professor Agis Iliadis, Chair/Advisor
Professor Martin Peckerar
Assistant Professor Kevin Daniels

Acknowledgements

ii. I would like to thank my advisor and Chair of the defense committee, Professor Agis Iliadis for his support and assistance in this research work. I would also like to thank the members of my defense committee, Professors Martin Peckerar and Kevin Daniels, for their helpful suggestions and comments.

Table of Contents

List of Tables

List of Figures

List of Abbreviations

SAW: Surface Acoustic Wave

IDT: Interdigital Transducer

CMOS: Complementary metal-oxide-semiconductor

UV: Ultraviolet

Introduction

ZnO and GaN are wide band gap semiconductors with significant electronic and piezoelectric properties [1]. They are promising materials for utilization in sensors [2-5] and UV light detecting devices [6]. ZnO and GaN have a considerable piezoelectric coefficient, so it allows the progress of surface acoustic wave applications. These two materials have been determined to have the possibility to work at high frequencies [7]. The manufacture of high-quality ZnO and GaN films on Si wafers and the improvement of SAW devices is very complicated, but it provides the benefit of integrated circuits with high-level CMOS technology for highly sensitive sensors. There are several reports displayed that high-quality ZnO and GaN films on Si wafers can be done by pulsed laser deposition and RF sputtering. Moreover, those devices were reported to operate at high frequency range.[8]

In recent years, SAW sensors have been widely used in acoustic, biological, and chemical equipment [9-12]. SAW devices also can be used for different types of acoustic waves with excellent sensitivities. A common type of acoustic wave propagation is Love mode propagation. The Love-mode waves are shear horizontal surface acoustic waves [12]. The advantage of this type of wave propagation is the acoustic energy of in-plane propagation is accumulated in the guiding layer. Therefore, it provides the chance of having high sensitivities. [13] Love mode of SAW is primary relying on the direction of the guiding layer film. It has minimal damping when the surface is contacted with liquid [14, 15]. Love mode devices using SiO_2 as the guiding layer have been tested previously, but the effect of SiO_2 has not been discussed.

In recent decades, ZnO is commonly used for manufacturing SAW sensors, but GaN has not been used as a general piezoelectric semiconductor for SAW sensors. However, GaN is actually an advanced semiconductor for diodes, transistors, and sensors due to extremely practical wide bandgap [24]. For example, GaN is successfully used to demonstrate a SAW sensor with high mass sensitivity for Lamb waves [25]. This sensor has a relatively high mass sensitivity, a small detecting area, and an excellent liquid resistance when comparing with other reported sensors with different semiconductors [25]. GaN is a piezoelectric semiconductor with many advantages for sensing, such as good acoustic velocity, and high thermal, chemical stability [25].

In this work, the parameters that affect sensitivity in SAW devices have been tested. The mass sensitivity can present how easy the acoustic wave can propagate in the device. Also, the comparison of the two materials was accomplished. One device is ZnO-based, and the other one is GaN-based. Thus, the differences between the two materials lead to instinct modeling results.

Love Mode SAW Sensor

In [1], ZnO/SiO_2/Si devices are examined. This modeling is based on the structure of the devices in [1]. The structure of the sensors is shown below in Fig. 1. The ZnO and GaN layers are wave guiding layer which can maintain the waves on the surface.

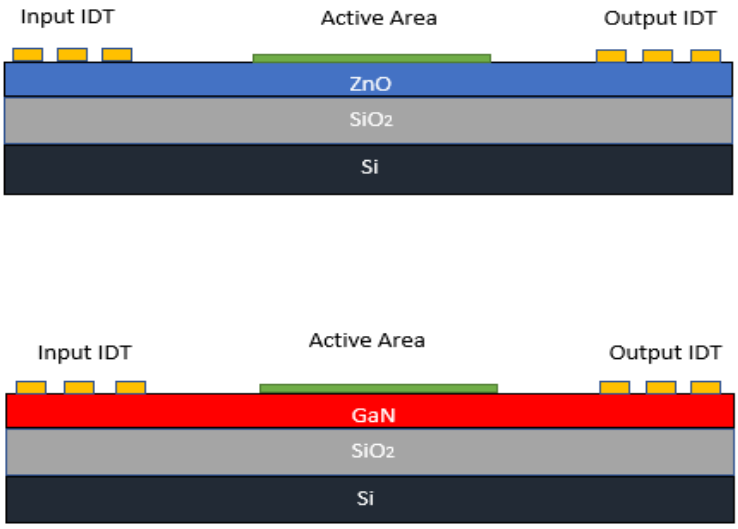

Figure 1: sectional view of the sensors

Acoustic waves in solid are produced by the movement of atoms in the piezoelectric substrate. When a piezoelectric material has applied a strain, the atoms in the material will be moved from their initial place. Meanwhile, the elastic force will tend to reestablish them [16]. This phenomenon causes the wave propagation that occurs at the surface of the substrate.

A general SAW sensor has two transducers that applied on the surface of the piezoelectric material. The transmitter is for generating the surface acoustic wave, and the receiver is for receiving the wave. The acoustic wave moves through the surface of the piezoelectric substrate, where the wave has been detected [17]. Figure 2(a) shows a normal SAW sensor, and 2(b) shows a SAW sensor with a wave guiding layer.

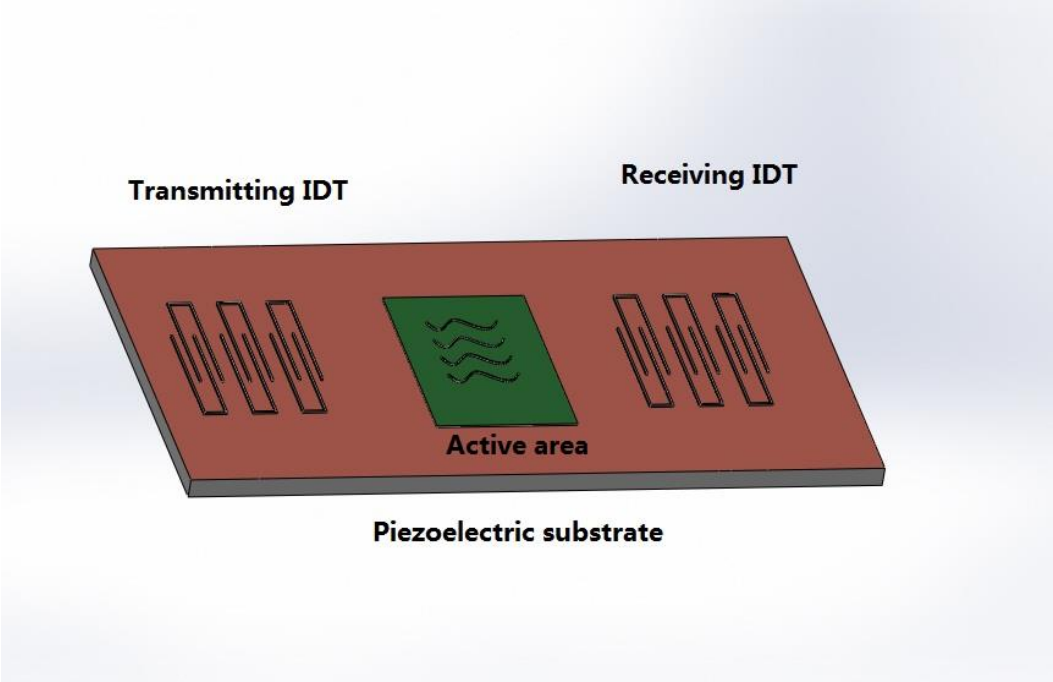

(a)

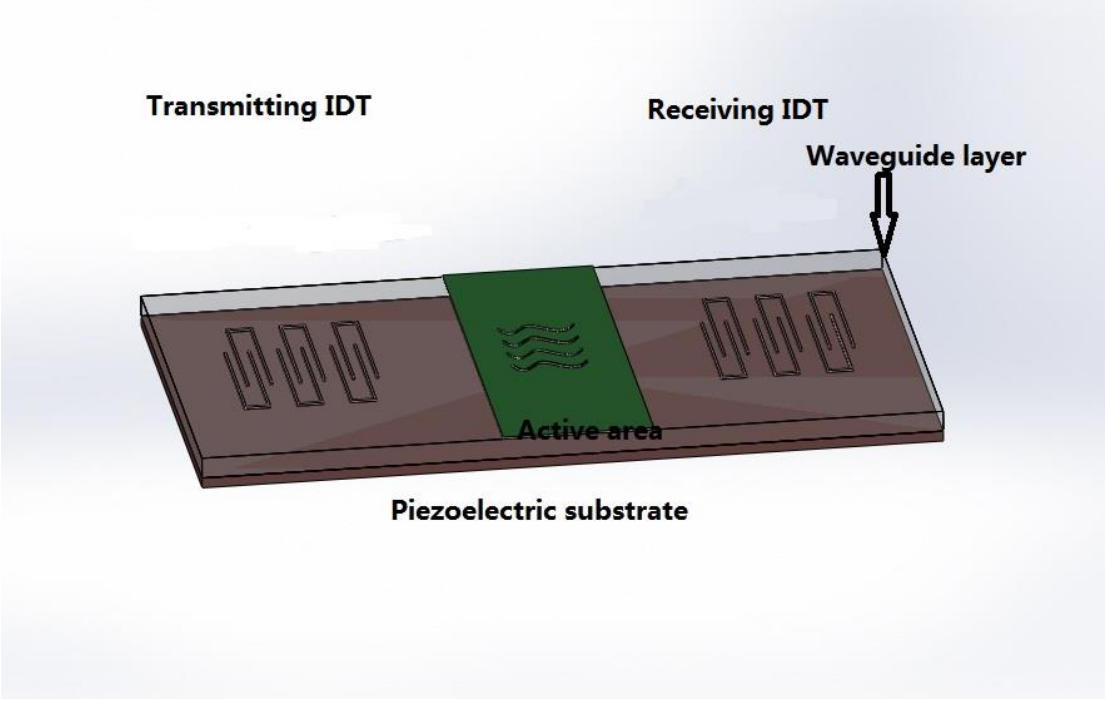

(b)

Figure 2 Schematic representations of a general two-port SAW sensor (a) and a wave-guided Love-mode SAW sensor (b).

If SAW sensors need a higher sensitivity, it is important to limit the acoustic energy near the surface of the sensor, and reduce wave spreading into the substrate [17, 23]. For this purpose, Love-mode SAW devices are well developed. The special characteristics of Love-mode devices is a guiding layer is used to restrict acoustic energy near the surface of the substrate. The waveguiding layer is made of a dielectric material, so it cannot transmit atoms. The surface acoustic waves are bounded to the interface because the surface waves are much slower than the wave in bulk [21]. Materials such as SiO_2, photoresist, parylene can be used as a proper guiding layer [18, 20].

Another important factor that can influence the detection sensitivity is the surface area of the active region. Large surface area can effectively absorb and release acoustic energy. Based on previous research, building nanostructure to the active region of the sensors can increase the surface area [17]. Thus, the research on the wave propagation on the nanostructured devices is necessary.

Modeling

This model is based on previous research that measured the mass sensitivity of Love-mode devices [1]. The basic equations are from [1]. The first important equation is as shown below. According to Krishnamoorthy and Iliadis [1], S_m^v is the mass sensitivity based on phase velocity; ρ_1 is the density of ZnO. v_1 is the shear velocity of the acoustic waves in ZnO, so v_1 = 4814 m/s; v_p is the shear velocity of the acoustic waves in the applied mass on the ZnO layer, and the material for the applied mass is polystyrene, so v_p is equal to 2400 m/s; v_0 is the operating point in on the

dispersion curve in the Love wave device with no mass loading; f_0 is the operating frequency of the Love wave device; z is the normalized guiding layer thickness (a dimensionless quantity) = d/λ = df_0/v$_l$, where $\lambda = v_1/f_0$, and d = actual thickness of ZnO film; v is the phase velocity of the acoustic waves along the direction of propagation [1]. This equation is used to build the plot that implies the relation between mass sensitivity and normalized guiding layer thickness.

$$S_m^v = \lim_{\Delta m \to 0} \frac{1}{\Delta m}\left(\frac{\Delta v}{v0}\right) = \frac{1}{\rho 1}\left[\frac{1-\frac{v_p^2}{v_0^2}}{1-\frac{v_l^2}{v_0^2}}\right]\frac{f_0}{v_l}\left(\frac{d\log_e v}{dz}\right) \quad (1)$$

From this equation, the mass sensitivity of certain material can be calculated based on operating frequency (f_0), the wavelength of the propagation wave (λ), and the thickness of the guiding layer (d) since z is equal to d/λ in the equation. Therefore, the first part of the modeling is to plot mass sensitivity vs. normalized guiding layer thickness with multiple wavelengths. The second part of the modeling is to find v_g / v, which implies the ratio between the group velocity (v_g) and the phase velocity (v). The equation of the ratio is as shown below. ρ_1 is the density, and d is the thickness of the guiding layer. S_m^v is the mass sensitivity calculated from Eq. (1). Eq. (2) shows that phase velocity will always be larger than group velocity.

$$\frac{V}{Vg} = 1 + \rho_1 * d * |S_m^v| \quad (2)$$

The next part of the model is to find S_m^f , the frequency-based mass sensitivity. S_m^f has a relation with S_m^v. The relation presents by Eq. (3) shown below. These two types of mass sensitivity are needed for comparison between different types of sensors.

$$S_m^f = \lim_{\Delta m \to 0} \frac{1}{\Delta m}\left(\frac{\Delta f}{f_0}\right) = \frac{Vg}{V} * S_m^v \quad (3)$$

The last part of this modeling is to plot the incremental rate of the mass sensitivity increases along with the wavelength. The equation used is shown below. When using Eq. (4), the thickness of the guiding layer (d) is a certain value, and the wavelength is the changing variable. In Eq. (4), the normalized guiding layer (z) is equal to d/λ, and d is a certain value, so it presents the relation between the incremental rate of mass sensitivity increases and the wavelength.

$$S_m^{v\prime} = \left(\frac{1}{\rho 1}\left[\frac{1-\frac{v_p^2}{v_0^2}}{1-\frac{v_l^2}{v_0^2}}\right]\frac{f_0}{v_l}\left(\frac{d\log_e v}{dz}\right)\right)', \quad (4)$$

This model evaluates the mass sensitivity based on the material, operation frequency (f_0), the wavelength of propagation wave (λ), the thickness of the guiding layer (d). It provides the function to find the best mass sensitivity with given conditions. The modeling is based on two types of materials which are ZnO, and GaN. Therefore, the test will make a comparison between the two types of devices.

The model is finished in MATLAB. The equations above are built in MATLAB and used to calculate the expected values. Those equations are also applied in the graphs to find the relations between the parameters and mass sensitivity. The modeling can approach a similar result with [1] as shown below in Fig. 3. Thus, this modeling can generate the ideal mass sensitivity based on the assigned parameters.

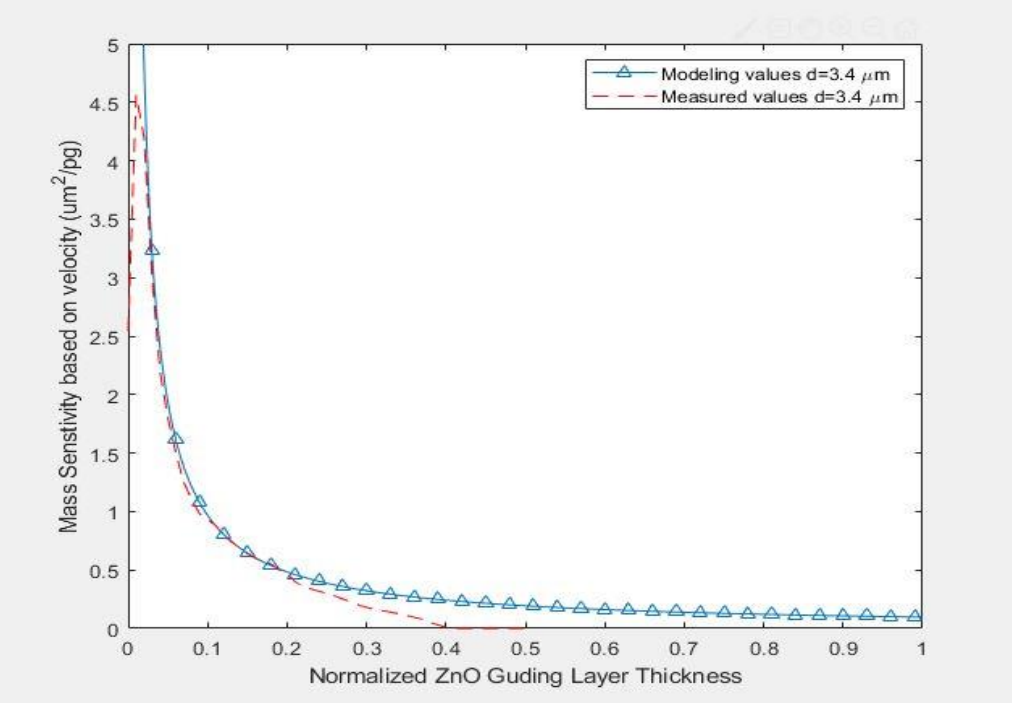

Figure 3: Comparison between measured values and modeling values

Result and Discussion

The evaluation of ZnO device was reported in [1] where the mass sensitivity of two ZnO devices at guiding layer thickness of 3.4 μm and 6.8 μm. Hence, the modeling starts with ZnO device. Fig. 4(a) shows the numerical mass sensitivity curve for ZnO devices. The value of mass sensitivity decreases along with z increases. This indicates that mass sensitivity can achieve higher value by reducing the guiding layer thickness. Moreover, the lines with larger wavelengths have a higher mass sensitivity, which implies increasing wavelength of the propagation wave can increase mass sensitivity. Fig. 4(b) shows the part of Fig. 4(a) when z is between 0 to 0.25. The maximum mass sensitivity is 3.6 μm^2/pg when λ = 6 μm. This matches the result from [1]. For calculating the increase rate of S_m^v from Fig. 4(b),

the thickness of the guiding layer is set to 3.4 µm. The incremental rate of S_m^v is increasing between each line. The increment starts at 0.0015 µm^2/pg and stops increasing at 0.29 µm^2/pg.

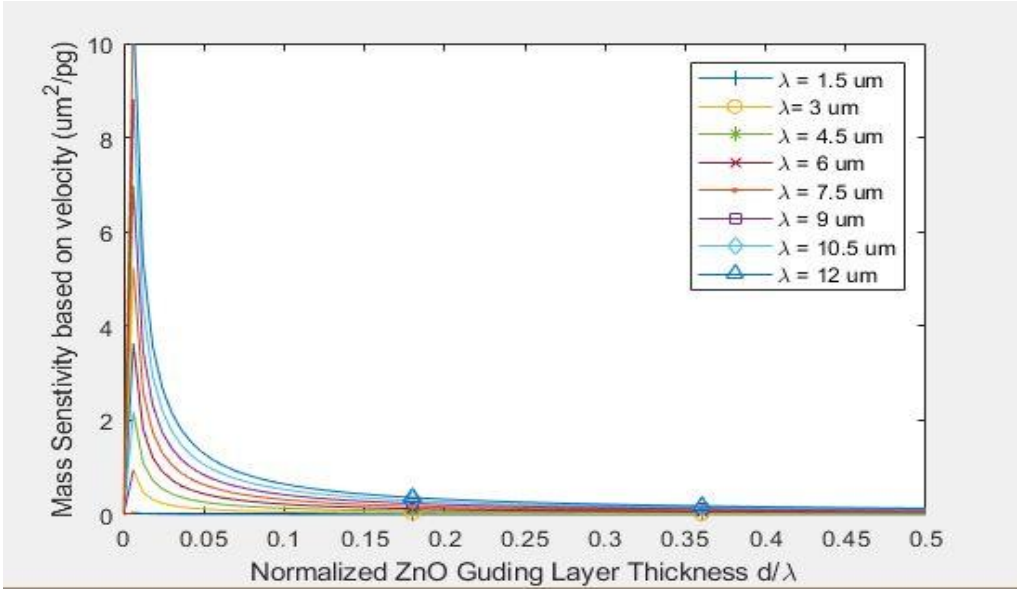

(a)

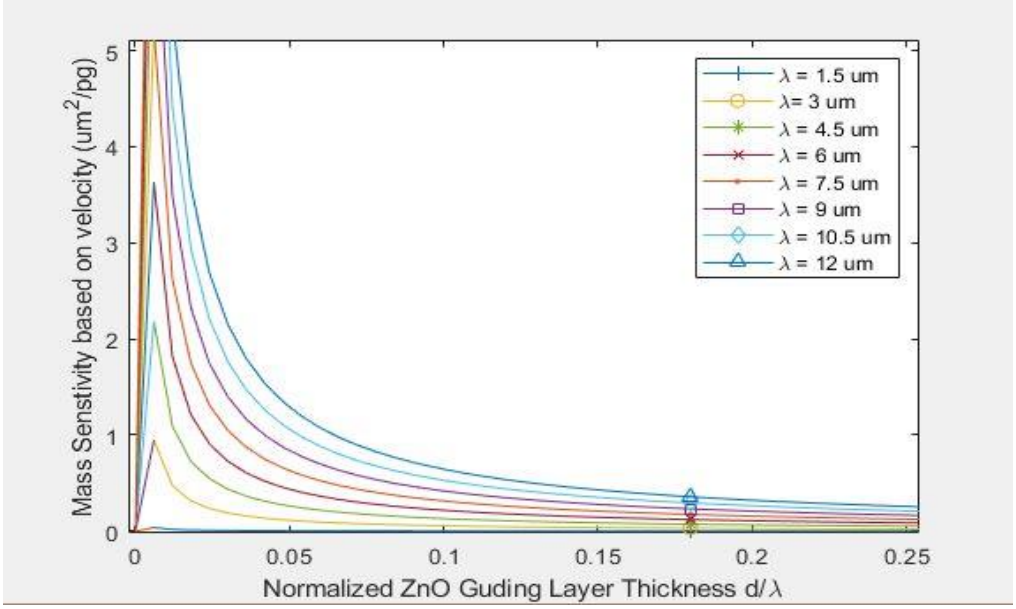

(b)

Figure 4 (a) Each line shows the velocity-based mass sensitivity for a ZnO-based device with different wavelengths. (b) The zoomed-in plot of (a) at z between 0 to 0.8.

As seen in Fig. 5, v_g / v is evaluated for each wavelength. v_g / v is the ratio of the group velocity to the phase velocity. From Eq. (3), S_m^v is calculated from the fractional change of phase velocity. Moreover, Eq. (5) shows that the fractional change of the frequency is related to the fractional change of phase velocity. Thus, the mass sensitivity that calculated from the fractional change of frequency, S_m^f, can be evaluated from Eq. 3.

$$\frac{\Delta f}{f0} = \left(\frac{Vg}{V}\right)\left(\frac{\Delta v}{V0}\right) \tag{5}$$

The value of v_g / v is decreasing when the wavelength is increasing, and it always less than one, which means the group velocity is always less than phase velocity. Moreover, v_g / v is used to calculate the frequency-based mass sensitivity in Eq. 3. Fig. 5 shows that v_g / v is inversely proportional to wavelength.

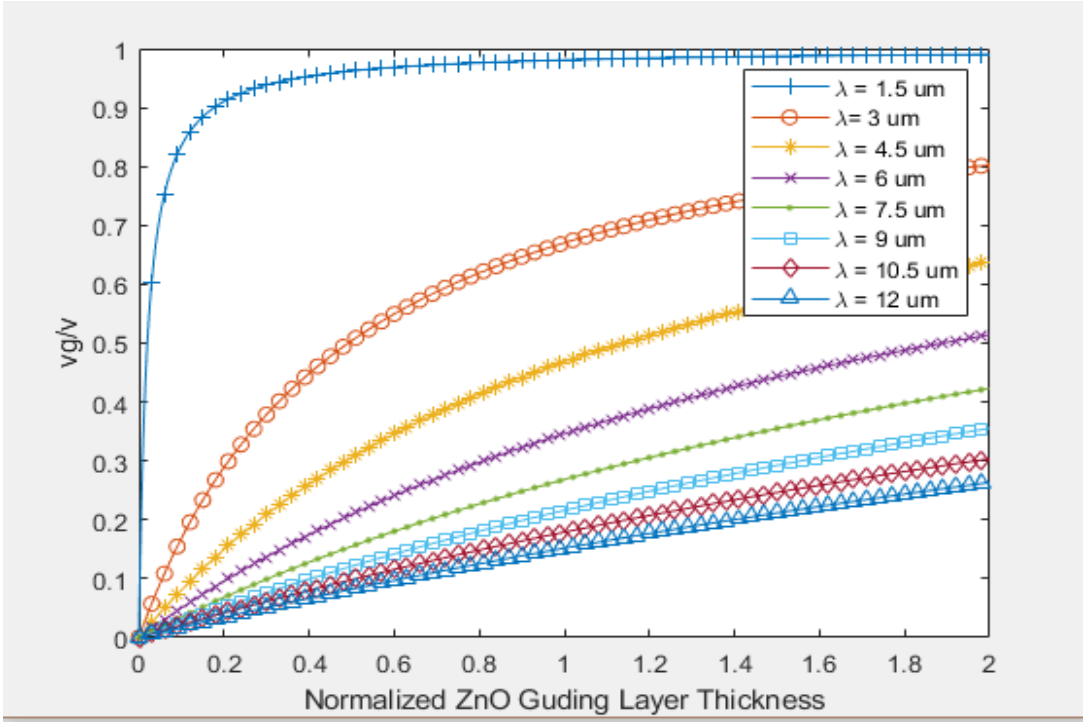

Figure 5 v_g / v for the ZnO-based device

Fig. 6 shows the frequency-based mass sensitivity, and it is proportional to v_g / v. Thus, S_m^f increases when the wavelength is increasing due to Eq. 3, but the increment of S_m^f between each line becomes smaller since v_g / v is decreasing. The maximum value of S_m^f is 3.4 μm^2/pg that approximately the same as the measured value of S_m^f in [1]. The incremental rate of S_m^f starts from 0.0215 μm^2/pg and ends increasing at 0.22 μm^2/pg.

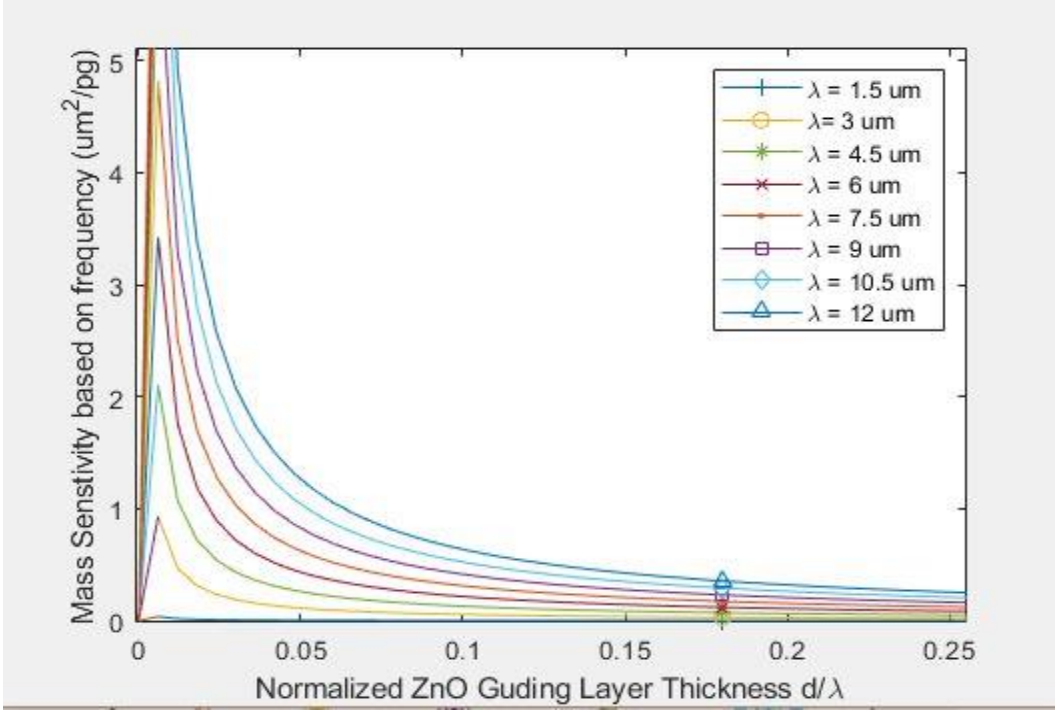

Figure 6 Frequency-based mass sensitivity with the ZnO-based device

Fig. 7 shows the first derivative of S_m^v with the chosen thickness of the guiding layer. It shows that the increment of S_m^v is not proportional. The rate of increase of S_m^v maintains the same after 10 μm. Fig. 7 has four lines with different thickness of the guiding layer, but they have the same trend that approaches to asymptotes. This matches the result from Fig.4. Based on the calculation from the curve in Fig. 7, the increase of the increment of velocity-based mass sensitivity is less than 2%.

Therefore, the incremental rate of S_m^v has an asymptote. It approximately keeps the same after 10 μm.

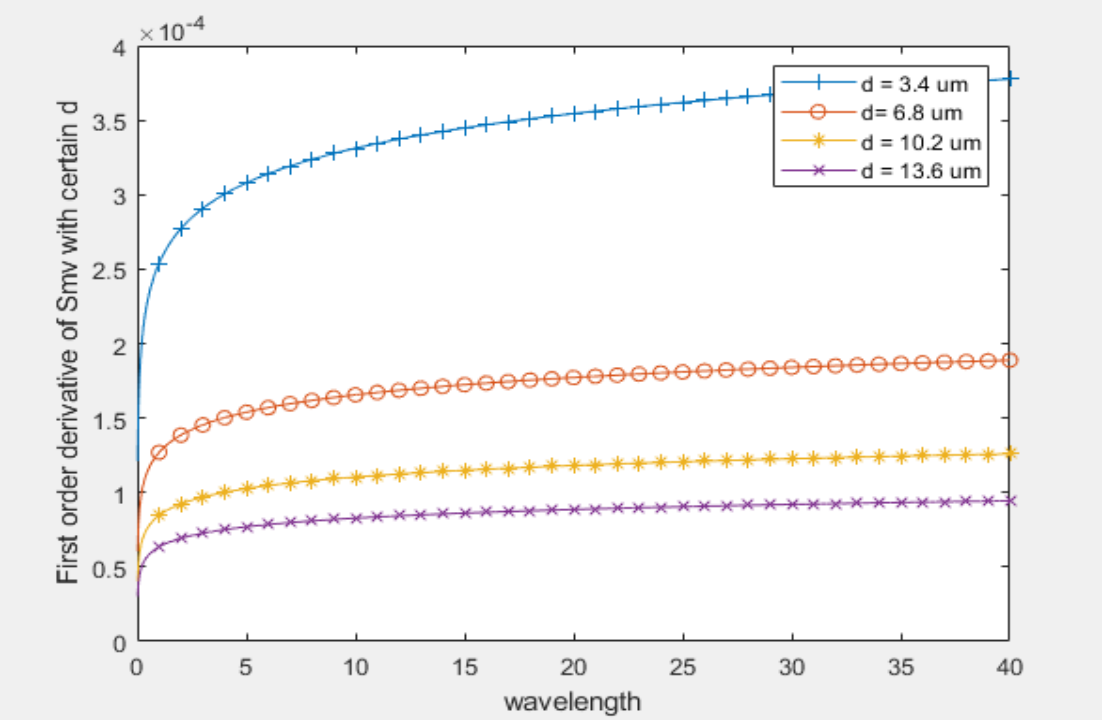

Figure 7 First derivative of S_m^v with different thickness of the guiding layer

The performance of sensors based on GaN is also evaluated. Fig. 8 shows the velocity-based mass sensitivity of the GaN devices. S_m^v of GaN devices has the same trend curve with the curve in Fig. 4 (a), but each line has higher values for the same z values. Based on the calculation from the curves, S_m^v of GaN devices is approximate 2.25 times higher than S_m^v of ZnO devices under the same wavelength and normalized guiding layer thickness. Fig. 8(b) shows the curves when z is between 0 to 0.25 from Figure. 8(a). The maximum mass sensitivity is 3.93 μm^2/pg when λ = 6 μm. For calculating the increase rate of S_m^v from Fig. 4(b), the thickness of the guiding layer is set to 3.4 μm. The incremental rate of S_m^v is rising between each wavelength. The rate starts from 0.0049 μm^2/pg and ends increasing at 0.67 μm^2/pg.

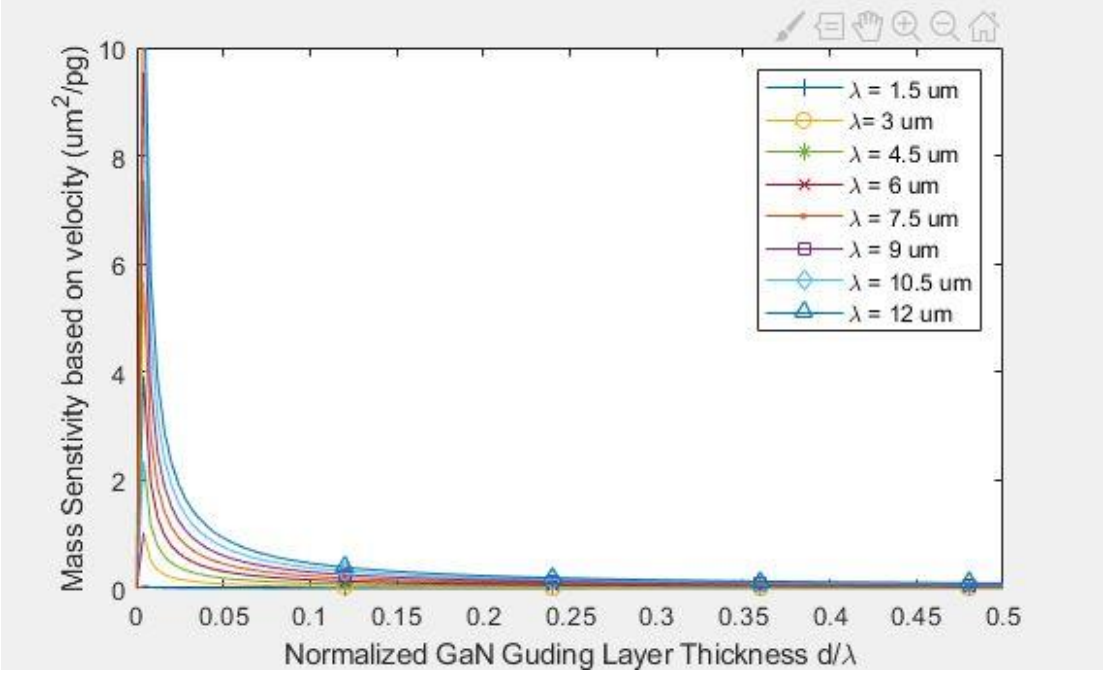

(a)

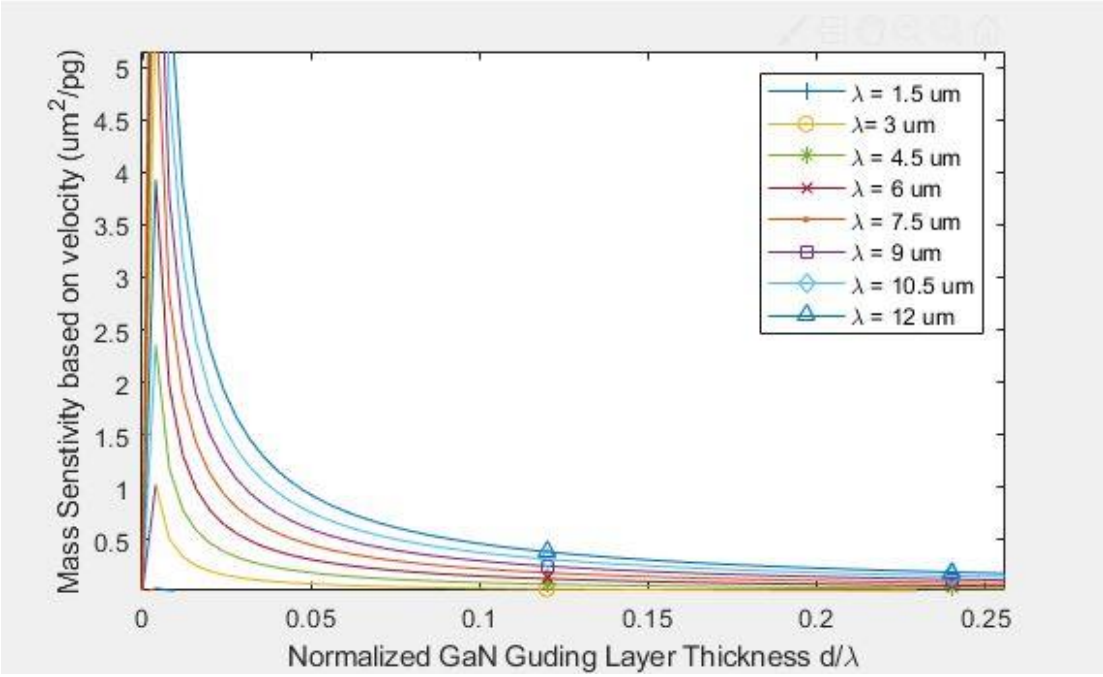

(b)

Figure 8 (a) Each line shows the velocity-based mass sensitivity for GaN-based device with different wavelengths. (b) The zoomed-in plot of (a) at z between 0 to 0.8.

The values of v_g / v for GaN devices, in general, are smaller than the values of ZnO devices. Based on Eq. 2, the reason is that the S_m^v of GaN devices is higher than ZnO devices. However, v_g / v in Fig. 9 still shows the group velocity is less than phase velocity for GaN devices, which means S_m^f of GaN devices will smaller than S_m^v due to Eq. 3.

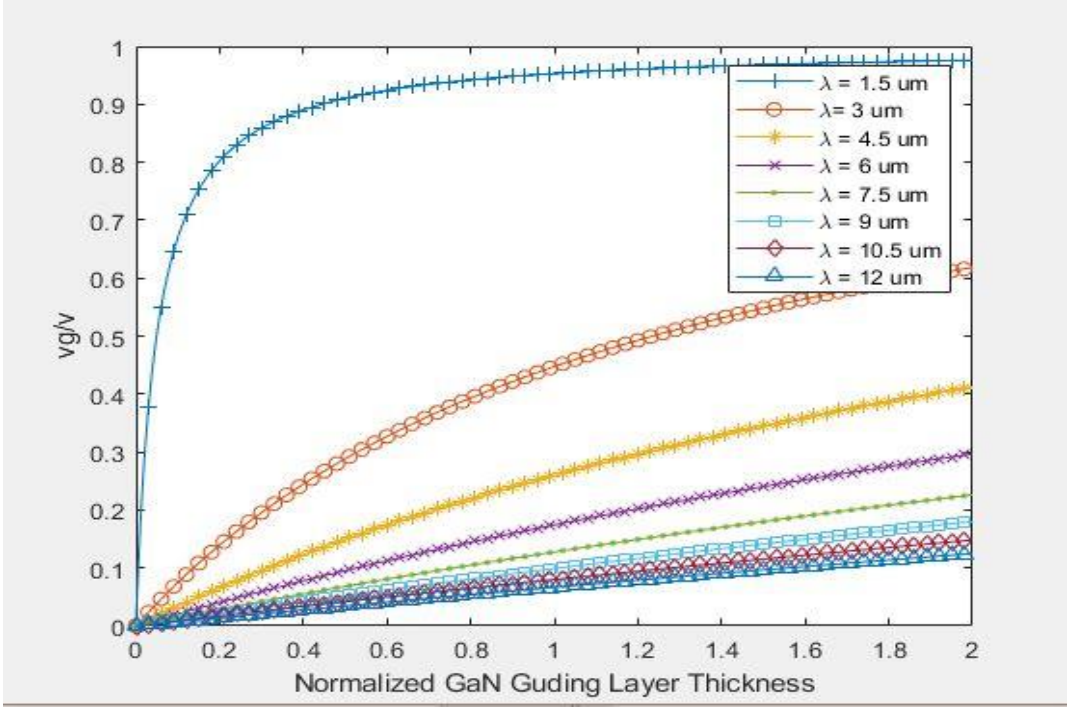

Figure 9 v_g / v for the GaN-based device

Fig. 10 shows the S_m^f of GaN devices. The curves have a similar trend with the curves in Fig. 6. Also, S_m^f increases when the wavelength is increasing due to the increase of S_m^v based on Eq. 3. The maximum value of S_m^f is 3.66 μm^2/pg, which is smaller than the maximum value of S_m^f in Fig. 4. Nevertheless, the overall values on the curve are higher than the S_m^f values of ZnO based devices. The incremental rate of S_m^f starts from 0.051 μm^2/pg and ends increasing at 0.33 μm^2/pg.

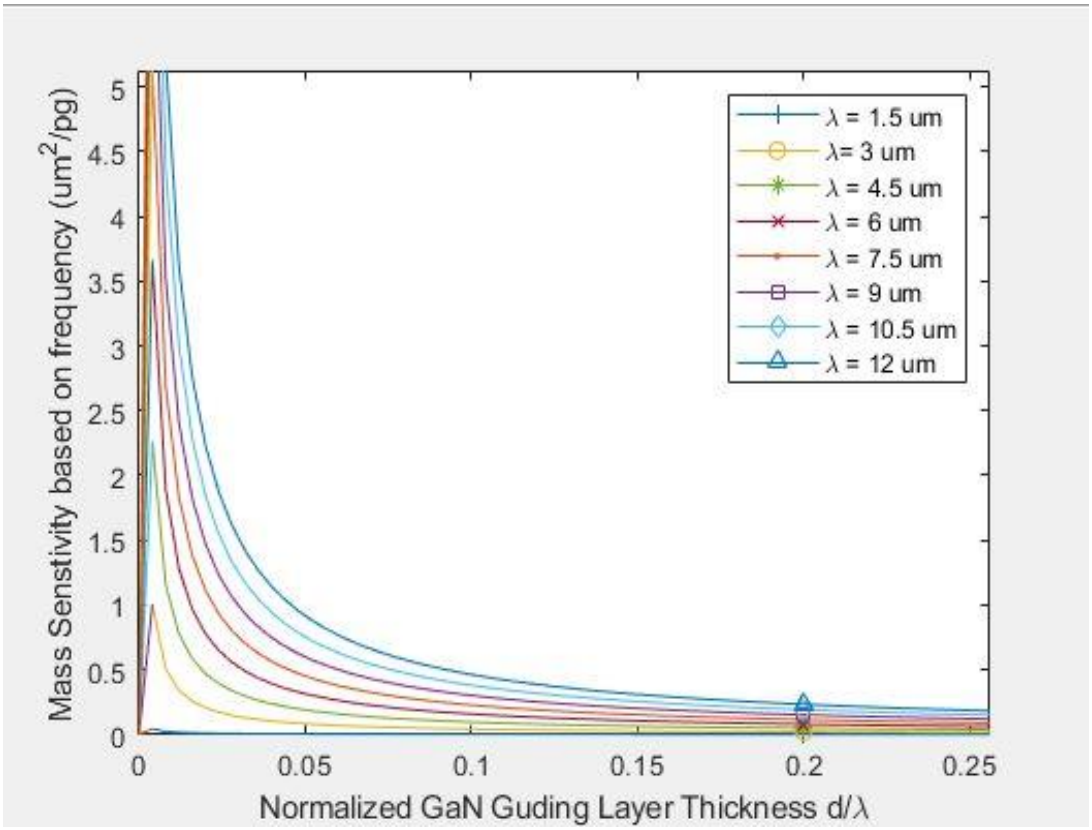

Figure 10 Frequency-based mass sensitivity with the GaN-based devices

Fig. 11 also displays the first derivative of GaN-based S_m^v with the selected thickness of the guiding layer. The increment of S_m^v is approaching to a limitation. This matches the result from Fig. 7. Moreover, the curve with a larger thickness of the guiding layer has a smaller limitation. The increment of S_m^v increase maintains the same after 10 μm.

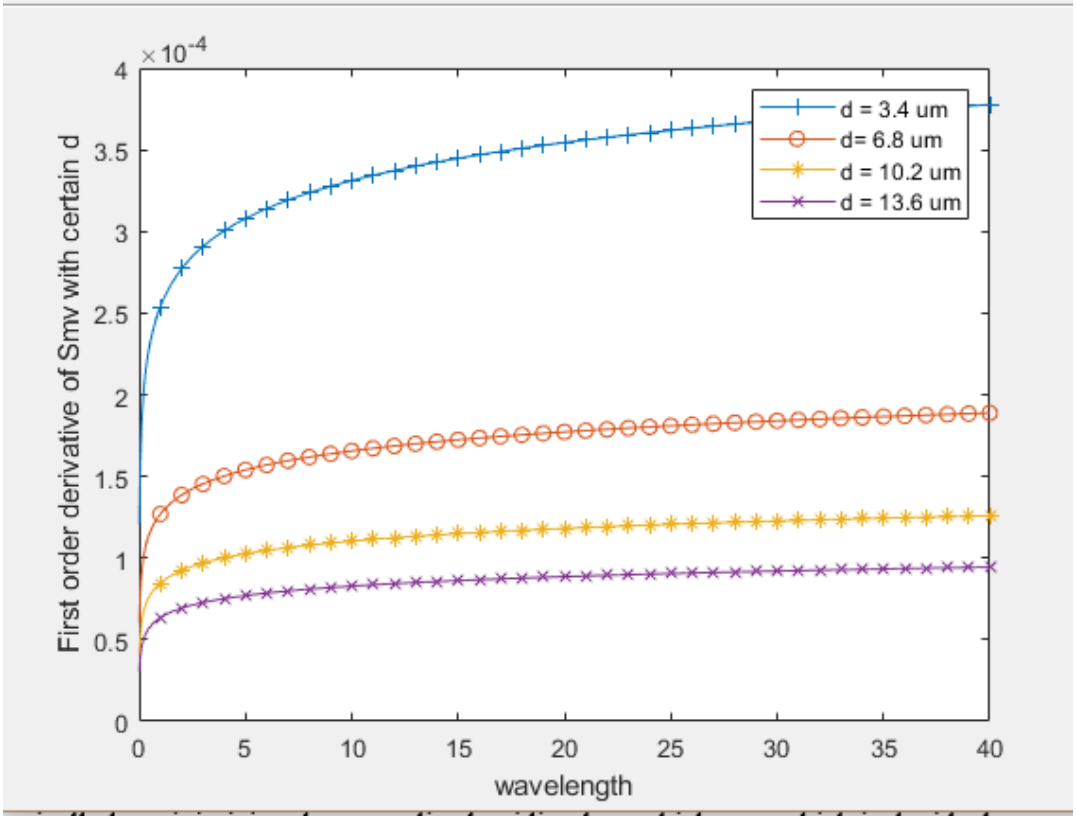

Figure 11 First derivative of S_m^v with different thickness of the guiding layer

When the conditions and parameters of the sensors are defined, the evaluation of the sensors is evaluated. From the evaluation, GaN-based devices have almost twice the sensitivity of ZnO-based devices with the same wavelength and thickness of the guiding layer. GaN-based devices have better performance than ZnO-based devices from the plots. Both S_m^v and S_m^f of GaN-based devices are higher. One reason that causes GaN devices performing better is the band gap of GaN is wider than ZnO.

The table below shows the maximum S_m^v for ZnO and GaN devices. It shows the S_m^v of GaN devices is approximate 10% better than GaN devices. The model displays the maximum mass sensitivity at d/λ = 0.05 which means the guiding layer thickness and wavelength can be selected for certain requirements.

ZnO Devices	Wavelength (μm)	1.5	3	4.5	6	7.5	9	10.5	12
	maximum S_m^v(μm^2/pg)	0.95	2.23	3.66	5.12	7.04	8.87	10.08	11.65
GaN Devices	Wavelength (μm)	1.5	3	4.5	6	7.5	9	10.5	12
	maximum S_m^v(μm^2/pg)	1.03	2.48	3.95	5.76	7.63	9.75	10.97	12.83

Table 1: The maximum S_m^v of ZnO and GaN devices.

Conclusion

The evaluation of the mass sensitivity is shown to match the result from [1] when the guiding layer thickness is 3.4 μm, and the wavelength is 6.8 μm. Therefore, this model can calculate mass sensitivity based on the chosen parameters. When the material, the thickness of guiding layer, and the wavelength are provided, the mass sensitivity of the sensor could be calculated. Moreover, the mass sensitivity increases along with wavelength increasing. Also, the incremental rate of mass sensitivity stopped increasing beyond λ = 10 μm, so the optimal wavelength should be above 10 μm. The mass sensitivity of the two devices increased dramatically with decreasing normalized guiding layer thickness. The comparison of the two different semiconductors ZnO and GaN, showed that the maximum mass sensitivity of GaN devices is 10% better than the maximum mass sensitivity of ZnO-based devices. The maximum of S_m^v appears at d/λ = 0.05, so the model can show a maximum mass sensitivity for a selected guiding layer thickness under multiple wavelengths. However, in practice defects in GaN epitaxial layers may reduce the mass sensitivity significantly. Coating GaN on different types of substrates causes the problem because the lattice structures of GaN usually cannot align [24]. When various displacements of atoms simultaneously occur, bonds between lattices strain and

finally crack [24]. Therefore, some planes of GaN lattices will permanently distort. This phenomenon causes the poor performance of GaN devices in practice.

Appendices

```
clear all;


p1 = 5.61;% density of ZnO
v1 = 4814; %the shear velocity of the acoustic waves in ZnO
vp = 2400;%the shear velocity of the acoustic waves in the applied mass on the ZnO layer
v0 = 4814.4; %v0 is the operating point in on the dispersion curve in the Love wave device with no mass loading
f0 = 0.708;%the operating frequency of the Love wave device
z = (0:0.006:2);%is the normalized guiding layer thickness =d/lamda
%z1 = [0.65:0.01:2];
z0 = 0.65;%the operating point of the dispersion curve
v = 4814.4; %the phase velocity of the acoustic waves along the direction of propagation =lamda*f0 lamda = 6.8
d =3.4; %m thicknees of guiding layer

lamda0 = 1.5;
for idx = 1:8
    lamda = lamda0 * idx;
    v = 0.708 * lamda;
    Smv = (1/p1)*((1-(vp^2/v0^2))/(1-(v1^2/v0^2)))*(f0/v1)*(d*log(v)./(d*z/lamda));
    Smv0(idx) = Smv(2);

    d1=3.4;
    vr1 = 1+p1*d1*abs(Smv);
    vri1 = (1./vr1);

    d2=3.4;
    vr2 = 1+p1*d2*abs(Smv);
    vri2 = (1./vr2);
    Smf1 = vri2.*Smv;
    Smf0(idx) = Smf1(2);
    marker = {'+','o','*','x','.','s','d','^'};

    figure(1)
%     xlim([0 0.5])
    ylim([0 10])

    plot(z,Smv,'marker', marker{idx},'markerindices', 1:30:length(Smv));
    xlim([0 0.5])
    hold on
    p(idx)= plot([0 0.006],[0 Smv0(idx)]);
    set(get(get(p(idx),'Annotation'),'LegendInformation'),'IconDisplayStyle','off');
    hold off
    xlabel('Normalized ZnO Guding Layer Thickness d/{\lambda}')
    ylabel('Mass Senstivity based on velocity (um^2/pg)')
    legend({'{\lambda} = 1.5 um','{\lambda}= 3 um','{\lambda} = 4.5 um','{\lambda} = 6 um','{\lambda} = 7.5 um','{\lambda} = 9 um','{\l
    hold all;

    figure(2)
    plot(z,vri1,'marker', marker{idx},'markerindices', 1:30:length(vri1));
    xlim([0 2])
    xlabel('Normalized ZnO Guding Layer Thickness d/{\lambda}')
    ylabel('vg/v')
    legend({'{\lambda} = 1.5 um','{\lambda}= 3 um','{\lambda} = 4.5 um','{\lambda} = 6 um','{\lambda} = 7.5 um','{\lambda} = 9 um','{\l
    hold on

    figure(3)
    plot(z,Smf1,'marker', marker{idx},'markerindices', 1:30:length(Smf1));
    xlim([0 0.5])
    hold on
    p2(idx)= plot([0 0.006],[0 Smf0(idx)]);
    set(get(get(p2(idx),'Annotation'),'LegendInformation'),'IconDisplayStyle','off');
    hold off
    xlabel('Normalized ZnO Guding Layer Thickness d/{\lambda}')
    ylabel('Mass Senstivity based on frequency (um^2/pg)')
```

```
    figure(3)
    plot(z,Smf1,'marker', marker{idx},'markerindices', 1:30:length(Smf1));
    xlim([0 0.5])
    hold on
    p2(idx)= plot([0 0.006],[0 Smf0(idx)]);
    set(get(get(p2(idx),'Annotation'),'LegendInformation'),'IconDisplayStyle','off');
    hold off
    xlabel('Normalized ZnO Guding Layer Thickness d/{\lambda}')
    ylabel('Mass Senstivity based on frequency (um^2/pg)')

    legend({'{\lambda} = 1.5 um','{\lambda}= 3 um','{\lambda} = 4.5 um','{\lambda} = 6 um','{\lambda} = 7.5 um','{\lambda} = 9 um','{\l
     hold on

end
hold off;

la = [0:0.01:40];
v=707.94*la;
d=3.4;
d1=6.8;
d2= 10.2;
d3= 13.6;

Smvd= (1/p1)*((1-(vp^2/v0^2))/(1-(v1^2/v0^2)))*(f0/v1)*(d*log(v)./(d.*d./la));
Smvd1= (1/p1)*((1-(vp^2/v0^2))/(1-(v1^2/v0^2)))*(f0/v1)*(d1*log(v)./(d1.*d1./la));
Smvd2= (1/p1)*((1-(vp^2/v0^2))/(1-(v1^2/v0^2)))*(f0/v1)*(d2*log(v)./(d2.*d2./la));
Smvd3= (1/p1)*((1-(vp^2/v0^2))/(1-(v1^2/v0^2)))*(f0/v1)*(d3*log(v)./(d3.*d3./la));
df = gradient(Smvd);
df1= gradient(Smvd1);
df2= gradient(Smvd2);
df3= gradient(Smvd3);

figure(4)
plot(la,df,'marker','+','markerindices',1:100:length(df));

ylabel('First order derivative of Smv with certain d');
xlabel('wavelength')

hold on
plot(la,df1,'marker','o','markerindices',1:100:length(df1));
plot(la,df2,'marker','*','markerindices',1:100:length(df2));
plot(la,df3,'marker','x','markerindices',1:100:length(df3));
legend({'d = 3.4 um','d= 6.8 um','d = 10.2 um','d = 13.6 um'},'Location','northeast')
hold off
```

```
clear all;

p1 = 6.15;% density of ZnO
v1 = 3766; %the shear velocity of the acoustic waves in ZnO
vp = 2400;%the shear velocity of the acoustic waves in the applied mass on the ZnO layer
v0 = 3766.4; %v0 is the operating point in on the dispersion curve in the Love wave device with no mass loading
f0 = 0.708;%the operating frequency of the Love wave device
z = [0:0.004:2];%is the normalized guiding layer thickness =d/lamda
v = 3766; %the phase velocity of the acoustic waves along the direction of propagation =lamda*f0 lamda = 6.8
d = 3.4; %um thicknees of guiding layer


lamda0 = 1.5;
for idx = 1:8
    %for z = [0:0.01:2]
    lamda = lamda0 * idx;
    v = 0.708 * lamda;
%     if z == 0,
%     Smv =0;
%     else
    Smv = (1/p1)*((1-(vp^2/v0^2))/(1-(v1^2/v0^2)))*(f0/v1)*(d*log(v)./(d*z/lamda));
    %end
%     end
    Smv0(idx) = Smv(2);

    d1=3.4;
    vr1 = 1+p1*d1*abs(Smv);
    vri1 = (1./vr1);

    d2=3.4;
    vr2 = 1+p1*d2*abs(Smv);
    vri2 = (1./vr2);
    Smf1 = vri2.*Smv;
    Smf0(idx) = Smf1(2);
    marker = {'+','o','*','x','.','s','d','^'};

    figure(5)
    xlim([0 2])
    ylim([0 10])

    plot(z,Smv,'marker', marker{idx},'markerindices', 1:30:length(Smv));
    xlim([0 0.5])
    hold on
    p(idx)= plot([0 0.004],[0 Smv0(idx)]);
    set(get(get(p(idx),'Annotation'),'LegendInformation'),'IconDisplayStyle','off');
    hold off
    xlabel('Normalized GaN Guding Layer Thickness d/{\lambda}')
    ylabel('Mass Senstivity based on velocity (um^2/pg)')
    ylim([0 10]);
    legend({'{\lambda} = 1.5 um','{\lambda}= 3 um','{\lambda} = 4.5 um','{\lambda} = 6 um','{\lambda} = 7.5 um','{\

    hold all;

    figure(6)
    plot(z,vri1,'marker', marker{idx},'markerindices', 1:50:length(vri1));
    xlim([0 2])
    xlabel('Normalized GaN Guding Layer Thickness d/{\lambda}')
```

```
    hold on

    figure(7)
    plot(z,Smf1,'marker', marker{idx},'markerindices', 1:50:length(Smf1));
    xlim([0 0.5])
    hold on
    p2(idx)= plot([0 0.004],[0 Smf0(idx)]);
    set(get(get(p2(idx),'Annotation'),'LegendInformation'),'IconDisplayStyle','off');
    hold off
    xlabel('Normalized GaN Guding Layer Thickness d/{\lambda}')
    ylabel('Mass Senstivity based on frequency (um^2/pg)')
    legend({'{\lambda} = 1.5 um','{\lambda}= 3 um','{\lambda} = 4.5 um','{\lambda} = 6 um','{\lambda} = 7.5 um','{\lambda} = 9 um','{\l
     hold on

end
hold off;



la = [0:0.01:40];

v=707.94*la;
d=1;
d1=0.5;
d2= 3;
d3= 4;
d4=5;
d5=9;
d6=10.5;
d7=12;

Smvd= (1/p1)*((1-(vp^2/v0^2))/(1-(v1^2/v0^2)))*(f0/v1)*(d*log(v)./(d.*d./la));
Smvd1= (1/p1)*((1-(vp^2/v0^2))/(1-(v1^2/v0^2)))*(f0/v1)*(d1*log(v)./(d1.*d1./la));
Smvd2= (1/p1)*((1-(vp^2/v0^2))/(1-(v1^2/v0^2)))*(f0/v1)*(d2*log(v)./(d2.*d2./la));
Smvd3= (1/p1)*((1-(vp^2/v0^2))/(1-(v1^2/v0^2)))*(f0/v1)*(d3*log(v)./(d3.*d3./la));
Smvd4= (1/p1)*((1-(vp^2/v0^2))/(1-(v1^2/v0^2)))*(f0/v1)*(d4*log(v)./(d4.*d4./la));
Smvd5= (1/p1)*((1-(vp^2/v0^2))/(1-(v1^2/v0^2)))*(f0/v1)*(d5*log(v)./(d5.*d5./la));
Smvd6= (1/p1)*((1-(vp^2/v0^2))/(1-(v1^2/v0^2)))*(f0/v1)*(d6*log(v)./(d6.*d6./la));
Smvd7= (1/p1)*((1-(vp^2/v0^2))/(1-(v1^2/v0^2)))*(f0/v1)*(d7*log(v)./(d7.*d7./la));
df = gradient(Smvd);
df1= gradient(Smvd1);
df2= gradient(Smvd2);
df3= gradient(Smvd3);
df4 = gradient(Smvd4);
df5 = gradient(Smvd5);
df6 = gradient(Smvd6);
df7 = gradient(Smvd7);
%df= (1/p1)*((1-(vp^2/v0^2))/(1-(v1^2/v0^2)))*(f0/v1)*((1+1./la)./d);

figure(8)
plot(la,df,'marker','+','markerindices',1:100:length(df));

ylabel('First order derivative of Smv with certain d');
xlabel('wavelength')

hold on
plot(la,df1,'marker','o','markerindices',1:100:length(df1));
plot(la,df2,'marker','*','markerindices',1:100:length(df2));
plot(la,df3,'marker','x','markerindices',1:100:length(df3));
plot(la,df4,'marker','.','markerindices',1:100:length(df4));
plot(la,df5,'marker','s','markerindices',1:100:length(df5));
plot(la,df6,'marker','d','markerindices',1:100:length(df6));
plot(la,df7,'marker','^','markerindices',1:100:length(df7));
legend({'d = 1.5 um','d= 3 um','d = 4.5 um','d = 6 um','d = 7.5 um','d = 9 um','d = 10.5 um','d = 12 um'},'Location','northeast')
hold off
```

References

[1] Soumya Krishnamoorthy and Agis Iliadis. Properties of high sensitivity zno surface acoustic wave sensors on sio2/(100) si substrates. Solid-State Electronics, 52:1710{1716, 11 2008.

[2] Sourajeet Roy and Sukumar Basu. Improved zinc oxide _lm for gas sensor applications. Bulletin of Materials Science, 25:513{515, 11 2002.

[3] Hongyan Xu, Xiulin Liu, Deliang Cui, Mei Li, and Minhua Jiang. A novel method for improving the performance of zno gas sensors. Sensors and Actuators B-chemical - SENSOR ACTUATOR B-CHEM, 114:301{307, 03 2006.

[4] Christos Pandis, ick Brilis, E. Bourithis, Dimitris Tsamakis, Hasina Ali, Sarayu Krishnamoorthy, Agis Iliadis, and Michael Kompitsas. Lowtemperature hydrogen sensors based on au nanoclusters and schottky contacts on zno _lms deposited by pulsed laser deposition on si and sio2 substrates. Sensors Journal, IEEE, 7:448 - 454, 04 2007.

[5] M.C. Horrillo, M.J. Fernndez, J.L. Fontecha, I. Sayago, M. Garca, Manuel Aleixandre, Javier Gutierrez, I. Grcia, and Carles Can. Optimization of saw sensors with a structure zno-sio2-si to detect volatile organic compounds. Sensors and Actuators B-chemical - SENSOR ACTUATOR B-CHEM, 118:356{361, 10 2006.

[6] Takayuki Makino, Chin-Hau Chia, Tuan Nguyen tien, Yoshihiko Segawa, M. Kavasaki, A. Ohmoto, K. Tamura, and H. Koimuma. Exciton spectra of zno epitaxial layers on lattice-matched substrates. Appl. Phys. Lett., 76, 01 2000.

[7] H. Nakahata, Satoshi Fujii, K Higaki, A. Hachigo, H Kitabayashi, Shin-ichi Shikata, and N Fujimori. Diamond-based surface acoustic wave devices. Semiconductor Science and Technology, 18:S96, 02 2003.

[8] Soumya Krishnamoorthy and A.A. Iliadis. Development of high frequency ZnO/SiO2/Si love mode surface acoustic wave devices. Solid-State Electronics, 50:1113{1118, 06 2006.18

[9] G. Bu, Michael Shur, D. Ciplys, Romualdas Rimeika, Remis Gaska, and Q. Fareed. Guided-wave acousto-optic di_raction in alxga1-xn epitaxial layers. Applied Physics Letters - APPL PHYS LETT, 85, 01 2004.

[10] E_e Howe and Geo_rey Harding. A comparison of protocols for the optimisation of detection of bacteria using a surface acoustic wave (saw) biosensor. Biosensors & bioelectronics, 15:641-9, 02 2000.

[11] Tsung-Lin Tsai and O.T.-C Chen. A piezoelectric sh-leaky saw biosensor for antibody detection. pages S1/59, 01 2005.

[12] R.L. Baer, C.A. Flory, M. Tom-Moy, and D.S. Solomon. Stw chemical sensors. pages 293 -298 vol.1, 11 1992.

[13] Jia Du, G. Harding, J. Ogilvy, P. Dencher, and M. Lake. A study of love-wave acoustic sensors sensors and actuators a. Sensors and Actuators A-physical - SENSOR ACTUATOR A-PHYS, 56:211{219, 09 1996.

[14] Cinzia Caliendo and Muhammad Hamidullah. A theoretical study of love wave sensors based on znoglass layered structures for application to liquid environments. Biosensors, 6:59, 12 2016.

[15] Falk Herrmann, Manfred Weihnacht, and S Buttgenbach. Temperature-compensated love mode sensors based on quartz/sio2 and litao3/sio2 systems. pages 180{187, 01 2001.

[16] B. Auld. Acoustic _elds and waves in solids. Physics Today, 27, 10 1974.

[17] Yeswanth Rao and Guigen Zhang. Enhancing the sensitivity of saw sensors with nanostructures. Current Nanoscience, 2:311{318, 11 2006.

[18] J.W. Gardner, Vijay Varadan, and Osama Awadelkarim. Microsensors, MEMS and Smart devices, pages 227{302. 11 2013.

[19] D.S. Ballantine, S.J. Martin, A.J. Ricco, G.C. Frye, H. Wohltjen, R.M. White, and E.T. Zellers. Chapter 3 - acoustic wave sensors and responses. In D.S. Ballantine, S.J. Martin, A.J. Ricco, G.C. Frye, H. Wohltjen, R.M. White, and E.T. Zellers, editors, Acoustic Wave Sensors, Applications of Modern Acoustics, pages 36 -149. Academic Press, Burlington, 1997.

[20] Muzar, Edward & Stotz, James. (2019). Surface acoustic wave modes in two-dimensional shallow void inclusion phononic crystals on GaAs. Journal of Applied Physics. 126. 025104. 10.1063/1.5056311..

[21] Ivan Lisenkov, R. Popov, and S. Nikitov. Acoustic wave propagation in uid metamaterial with solid inclusions. Applied Physics A, 103:921{925, 06 2011. 19

[22] Jin-Chen Hsu and Tsung-Tsong Wu. Bleustein-gulyaev-shimizu surface acoustic waves in two-dimensional piezoelectric phononic crystals. IEEE Transactions on Ultrasonics, Ferroelectrics, and Frequency Control, 53(6):1169{1176, June 2006.

[23] Guigen Zhang. Nanostructure-enhanced surface acoustic waves biosensor and its computational modeling. Journal of Sensors, 2009, 08 2009.

[24] Giaremis S, Komninou P, Belabbas I, Chen J and Kioseoglou J. Structural and electronic properties of *a*-edge dislocations along ⟨1-100⟩ in GaN. 2018 J. Appl. Phys. 123 244301

[25] X. Lu, C. M. Lee, S. Y. Wu, H. P. Ho and K. M. Lau, "GaN-Based S0 -Wave Sensors on Silicon for Chemical and Biological Sensing in Liquid Environments," in *IEEE Sensors Journal*, vol. 13, no. 4, pp. 1245-1251, April 2013. doi: 10.1109/JSEN.2012.2231958